Available online at www.sciencedirect.com
SCIENCE DIRECT
Journal of Sound and Vibration 297 (2006) 444–455
JOURNAL OF SOUND AND VIBRATION
www.elsevier.com/locate/jsvi

Letter to the Editor

# Dynamics of satellite separation system

D. Jeyakumar[a], B. Nageswara Rao[b,*]

[a]*Mission Design and Analysis Division, Launch Vehicle Design Entity, Vikram Sarabhai Space Centre, Thiruvananthapuram 695 022, India*
[b]*Structural Analysis and Testing Group, Aeronautics Entity, Vikram Sarabhai Space Centre, Thiruvananthapuram 695 022, India*

Received 19 January 2004; received in revised form 23 March 2006; accepted 27 March 2006
Available online 5 June 2006

**Abstract**

This paper presents the coordinate systems; coordinate transformations and equations of motion useful for the design and analysis of satellite separation system using the helical compression spring mechanism. A fourth-order Runge–Kutta method is adopted to solve the non-linear ordinary differential equations of motion to obtain the 12 degrees of freedom for the separating bodies, for the specified dynamic parameters. A reliable statistical approach is followed to account the variations in the specified dynamic parameters. The tolerances in the magnitude of the body rates, relative velocity and relative distance between the separating bodies are presented for use in the design to achieve the desired separation system.
© 2006 Elsevier Ltd. All rights reserved.

## 1. Introduction

The long-range ballistic missile (with its warhead), artificial satellite, and spacecraft use a multistage rocket as their carrier. Due to the fact that separation between stages during the flight of a multistage rocket can cast off, in sequence, the stage in which the propellants have been exhausted, the weight of the final stage at ignition is considerably reduced. Thus, the guided missile and spacecraft can attain a relatively high and necessary velocity. Therefore, separation between stages in a multistage carrier rocket is an important problem to solve for a successful launch of a ballistic missile, artificial satellite or spacecraft.

The separation events are often mission critical. Any mechanical interference between the separating bodies is likely to be catastrophic. The launch failures of Atlas Centaur in 1970 and Chinese Long March in 1992, improper placing of satellite orbits of Titan in 1990, Pegasus in 1991, and Delta-2 in 1995 are some of the typical examples wherein faulty separation systems were suspected to be the main culprits. A judicious separation system design not only ensures a collision-free separation, but also limits the resulting disturbance to the on-going stage to a minimum. A typical launch mission may involve several separation events such as the stage separation, the strap-on separation, the heat shield separation, the ullage rocket separation and the spacecraft separation. The dynamics of separating bodies has received the attention of several investigators [1–23].

The separation of spacecraft components, which occur in every flight, represents crucial and major events that must be successfully executed to fulfill mission requirements. Separation systems vary as widely in

*Corresponding author. Tel.: +91 471 2565640; fax: +91 471 2704134.
*E-mail address:* bnrao52@rediffmail.com (B.N. Rao).

0022-460X/$ - see front matter © 2006 Elsevier Ltd. All rights reserved.
doi:10.1016/j.jsv.2006.03.035

**Nomenclature**

| | |
|---|---|
| $A_z$ | launch azimuth (deg) |
| $\mathbf{F}_{\text{ext}} =$ | $(\mathbf{F}_g+\mathbf{F}_S)$ total external force due to gravity and spring system (N) |
| $h$ | altitudeof separation (m) |
| $I$ | inertia tensor |
| $t$ | time (s) |
| $m_M$, $m_S$ | mass of the ongoing and spent bodies (kg) |
| $\mathbf{M}_{\text{ext}} =$ | $(\mathbf{M}_g+\mathbf{M}_S)$ total external moment (Nm) |
| $R_E$, $R_P$, $R_S$ | Earth's equatorial radius, polar radius, radius at the surface (m) |
| $r$, $q$, $p$ | body rates yaw, pitch and roll |
| $\mathbf{r}_I$ | position vector in ECI frame (m) ($X_I$, $Y_I$, $Z_I$) |
| $\mathbf{r}_{\text{CG}}$ | position vector of the body CG offset (m) |
| $r_s$ | spring location from CG (m) |
| $v$ | velocity in the body frame (m/s) |
| $X$, $Y$, $Z$ | body axes yaw, pitch and roll |
| $\psi,\theta,\phi$ | yaw, pitch and roll attitude angles w.r.t LPI frame (deg) |
| $\Phi_{\text{GC}}$ | geocentric latitude of the launch station (deg) |
| $\Phi_{\text{GD}}$ | geodetic latitude of the launch station (deg) |
| $\Theta$ | launch station longitude (deg) |
| $\mu$ | Earth's gravitational constant ($m^3/s^2$) |
| $\Omega_E$ | Earth's angular velocity (rad/s) |
| $\delta$ | spring mounting azimuth angle (deg) |
| $\kappa$ | spring stiffness (N/m) |
| $\xi$ | stroke length (m) |

physical and functional properties as the performance requirements, which they must satisfy; however, most systems use helical compression springs as an energy source.

This paper presents a mathematical formulation for the analysis of satellite separation system using the helical compression spring mechanism. The problem is modeled under the influence of forces and moments of the individual bodies undergoing separation, treating the bodies as rigid. The bodies undergoing separation have 12 degrees of freedom (dof), viz., three velocity vectors, three position vectors, three body rates and three body attitude angles. The different coordinate systems required for the space dynamics of separating bodies are: geocentric inertial or Earth centered inertial (ECI) frame; topo-centric or launch point inertial (LPI) frame; Body coordinate system; and local inertial or common body inertial (CBI) frame. In principle equations of motion can be solved in any coordinate system. It is advantageous to solve them in the body coordinate system, as the moment of inertia, engine tail-off thrust and aerodynamic computations are very simple in the body coordinate system while gravity computation is simpler in geo centric inertial coordinate system. Transformation from one coordinate frame to another is made in the present study as the forces and moments are defined in different coordinate systems. The non linear ordinary differential equations of motion are solved for a typical satellite separation system using a fourth-order Runge–Kutta integration scheme. Collision-free separation assessment is possible from the gap (distance) between the pair of points at critical locations in the separating bodies.

## 2. Formulation

The physical problem is to simulate the dynamic characteristics of the separating rigid bodies under the influence of forces and moments acting on them. Each individual body has three velocity components, three components of position vector, three body rates and three attitude angles, respectively. In principle, equations of motion can be solved in any coordinate system. It is preferable to solve them in the body coordinate system, as the moment of inertia, engine tail off thrust and aerodynamic computations are very simple in the body coordinate system. Figs. 1 and 2 show the different coordinate frames used in the present study. The $X_I$, $Y_I$, and $Z_I$ axes as shown in Fig. 1 define the ECI coordinate system. The axes $X_I$ and $Y_I$ lie in the equatorial plane and $Z_I$ pointing towards North Pole. Gravitational forces are computed in this coordinate system. The $X_T$, $Y_T$, and $Z_T$ axes define the topo-centric or LPI coordinate system. The ECI and LPI coordinates are related through the launch azimuth ($A_z$), launch site geocentric latitude ($\Phi_{\text{GC}}$) and launch site longitude ($\Theta$). The vehicle orientation at any time is defined with the Euler angles, viz., yaw attitude angle ($\psi$), pitch attitude angle ($\theta$), and roll attitude angle ($\phi$) with respect to LPI frame. The body frame coincides with LPI frame at the time of launch. It has its origin at the center of gravity (CG) of the individual bodies, namely main (ongoing) body

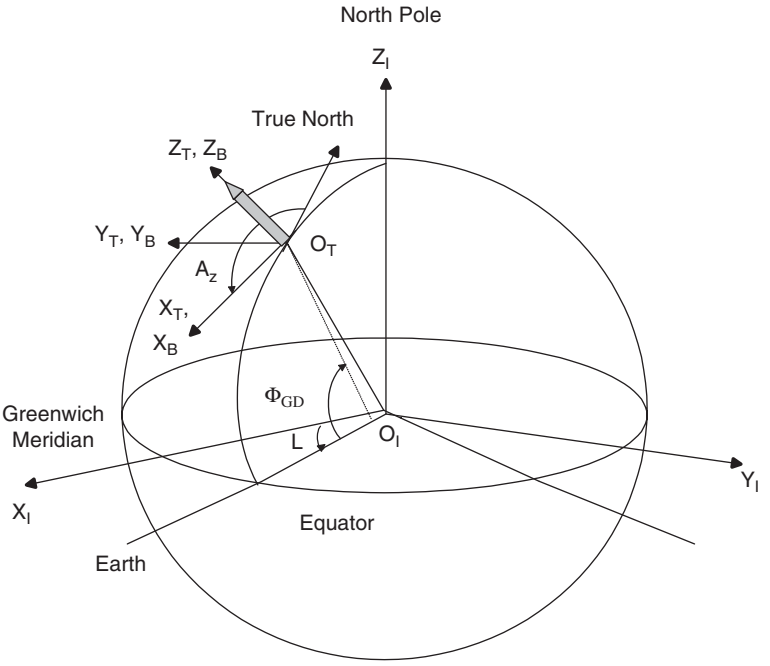


Fig. 1. Earth centered inertial and launch point inertial frames.

and separating (spent) body as shown in Fig. 2. The $X_M$, $Y_M$ and $Z_M$ axes with $M_{CG}$ as origin define the main body coordinate system. The $X_S$, $Y_S$ and $Z_S$ axes with $S_{CG}$ as origin define the separating body coordinate system. The $X_L$, $Y_L$ and $Z_L$ axes coincide with body axes of the combined body just before separation. This frame moves with a constant velocity same as that of the combined body at the instant of separation.

### 2.1. Equations of motion

Consider a space vehicle with a set of body fixed axes $X$, $Y$, and $Z$ rotating with angular velocity $\boldsymbol{\omega}$, and with the origin coinciding with the center of gravity of the vehicle. The translational and rotational equations of motion for each body in the respective body frame are

$$m\left\{\frac{\mathrm{d}\mathbf{v}}{\mathrm{d}t}\right\} + m\boldsymbol{\omega} \times \mathbf{v} = \mathbf{F}_{\text{ext}}, \tag{1}$$

$$\frac{\mathrm{d}\mathbf{L}}{\mathrm{d}t} + \boldsymbol{\omega} \times \mathbf{L} = \mathbf{M}_{\text{ext}}. \tag{2}$$

Here $m$ is the mass of the body, $\mathbf{v} = v_x\mathbf{i}_b + v_y\mathbf{j}_b + v_z\mathbf{k}_b$, is the velocity, $\boldsymbol{\omega} = r\mathbf{i}_b + q\mathbf{j}_b + p\mathbf{k}_b$, is the angular velocity, which has components $r$, $q$ and $p$ along the body axes, viz., yaw, pitch and roll, respectively, $t$ is time, $\mathbf{F}_{\text{ext}} = F_x\mathbf{i}_b + F_y\mathbf{j}_b + F_z\mathbf{k}_b$, is the total external force vector, $\mathbf{L} = L_x\mathbf{i}_b + L_y\mathbf{j}_b + L_z\mathbf{k}_b$, is the angular momentum vector, $\mathbf{M}_{\text{ext}} = M_x\mathbf{i}_b + M_y\mathbf{j}_b + M_z\mathbf{k}_b$, is the total external moment vector. $\mathbf{i}_b, \mathbf{j}_b, \mathbf{k}_b$ are the unit vectors with respect to the center of mass of the respective body frame.

The components of angular momentum vector are obtained from

$$\begin{Bmatrix} L_x \\ L_y \\ L_z \end{Bmatrix} = [I]\begin{Bmatrix} r \\ q \\ p \end{Bmatrix} = \begin{bmatrix} I_{xx} & -I_{xy} & -I_{xz} \\ -I_{yx} & I_{yy} & -I_{yz} \\ -I_{zx} & -I_{zy} & I_{zz} \end{bmatrix}\begin{Bmatrix} r \\ q \\ p \end{Bmatrix}. \tag{3}$$

Here $I_{xx}$, $I_{yy}$ and $I_{zz}$ are the principal moment of inertia about yaw, pitch and roll ($X$, $Y$, $Z$) axes respectively. $I_{xy}$, $I_{xz}$, $I_{yx}$, $I_{yz}$, $I_{zx}$ and $I_{zy}$ are the product of inertia with respect to the indicated planes, e.g.,

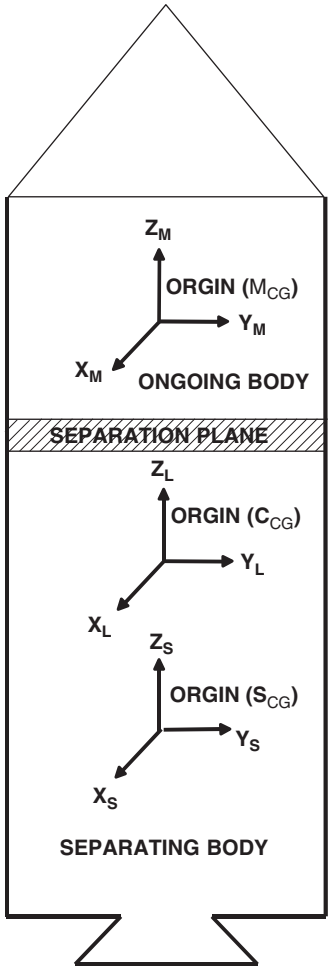


Fig. 2. Body and local inertial coordinate systems.

$xy$, $xz$, $yz$. The symmetry in the products of inertia has been noted. It may be noted that the principal moments of inertia may only be positive, but the products of inertia may be either positive or negative.

Eqs. (1) and (2) can be written in the form

$$\frac{\mathrm{d}}{\mathrm{d}t}\begin{Bmatrix} v_x \\ v_y \\ v_z \end{Bmatrix} = \begin{Bmatrix} pv_y - qv_z \\ rv_z - pv_x \\ qv_x - rv_y \end{Bmatrix} + \frac{1}{m}\begin{Bmatrix} F_x \\ F_y \\ F_z \end{Bmatrix}, \tag{4}$$

$$\frac{\mathrm{d}}{\mathrm{d}t}\begin{Bmatrix} r \\ q \\ p \end{Bmatrix} = [I]^{-1}\begin{Bmatrix} pL_y - qL_z + M_x \\ rL_z - pL_x + M_y \\ qL_x - rL_y + M_z \end{Bmatrix}. \tag{5}$$

The kinematic differential equations, which provide the relationship between Euler angles and angular velocity components (body rates) are

$$\frac{\mathrm{d}}{\mathrm{d}t}\begin{Bmatrix} \psi \\ \theta \\ \phi \end{Bmatrix} = \begin{bmatrix} \cos\phi & -\sin\phi & 0 \\ \sin\phi\sec\psi & \cos\phi\sec\psi & 0 \\ \sin\phi\tan\psi & \cos\phi\tan\psi & 1 \end{bmatrix}\begin{bmatrix} r \\ q \\ p \end{bmatrix}. \tag{6}$$

Eqs. (4)–(6) are the governing equations of motion for the individual bodies undergoing separation and are nonlinear ordinary differential equations, which are to be solved numerically after specifying the components of total external force and moment vectors. The dynamic characteristics of the separating bodies are modeled here under the influence of the gravity and the spring forces and moments.

### 2.2. Gravity force and moment

The gravitational acceleration along the ECI frame is computed as

$$\mathbf{g}_{\mathrm{EC}} = g_{XI}\mathbf{e}_x + g_{YI}\mathbf{e}_y + g_{ZI}\mathbf{e}_z = -\mathrm{grad}\, U, \tag{7}$$

where the gravitational potential

$$U = -\frac{\mu}{r_I}\left[1 - \frac{1}{2}J_2\eta^2\left(3\zeta^2 - 1\right) - \frac{1}{2}J_3\eta^3\left(5\zeta^3 - 3\zeta\right) - \frac{1}{8}J_4\eta^4\left(35\zeta^4 - 30\zeta^2 + 3\right)\right], \tag{8}$$

$$\eta = \frac{R_E}{r_I}, \quad \zeta = \frac{Z_I}{r_I}, \quad \mathbf{r}_I = X_I\mathbf{e}_x + Y_I\mathbf{e}_y + Z_I\mathbf{e}_z,$$

is the vehicle position vector with respect to the ECI frame; $r_I = \sqrt{\mathbf{r}_I \cdot \mathbf{r}_I}$, is the radial distance of the vehicle from the earth center, $R_E$ is the equatorial radius of the oblate Earth geometry (see Fig. 3). The gravitational constant, $\mu = 3.9860253 \times 10^{14}\,\mathrm{m}^3/\mathrm{s}^2$; gravitational harmonics $J_2 = 1.0827 \times 10^{-3}$; $J_3 = -2.3 \times 10^{-6}$; $J_4 = -1.8 \times 10^{-6}$.

Since the gravitational acceleration (7) is computed in ECI frame, it has to be transformed to the LPI frame. The transformation matrix $[T_{\mathrm{EL}}]$ which transfers the components of a vector from ECI frame to LPI frame, is

$$[T_{\mathrm{EL}}] = \left\{e_{ij}\right\}_{3\times 3}, \tag{9}$$

where

$$\begin{aligned} e_{11} &= -\cos A_z \sin \Phi_{\mathrm{GC}} \cos \Theta - \sin A_z \sin \Theta, \\ e_{12} &= -\cos A_z \sin \Phi_{\mathrm{GC}} \sin \Theta + \sin A_z \cos \Theta, \\ e_{13} &= \cos A_z \cos \Phi_{\mathrm{GC}}, \end{aligned}$$

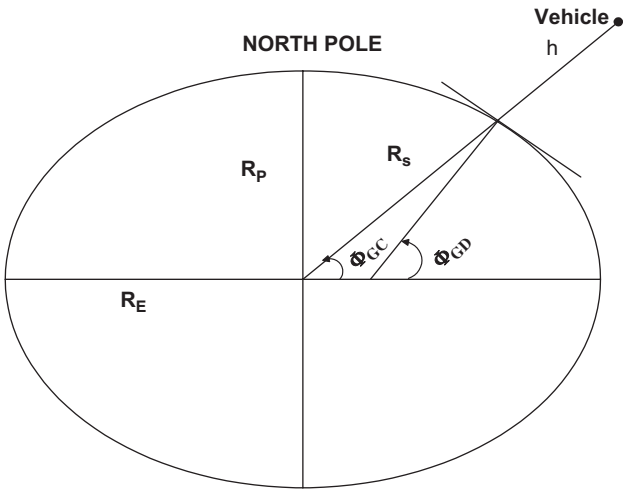


Fig. 3. Oblate earth geometry.

$$
\begin{aligned}
e_{21} &= -\sin A_z \sin \Phi_{GC} \cos \Theta + \cos A_z \sin \Theta,\\
e_{22} &= -\sin A_z \sin \Phi_{GC} \sin \Theta - \cos A_z \cos \Theta,\\
e_{23} &= \sin A_z \cos \Phi_{GC},\\
e_{31} &= \cos \Phi_{GC} \cos \Theta,\\
e_{32} &= \cos \Phi_{GC} \sin \Theta,\\
e_{33} &= \sin \Phi_{GC}.
\end{aligned}
$$

The geocentric latitude of the vehicle position is $\Phi_{GC} = \sin^{-1}(Z_I/r_I)$, the geodetic latitude of the vehicle position is $\Phi_{GD} = \tan^{-1}\left\{(R_E/R_P)^2 \tan \Phi_{GC}\right\}$, $R_P$ is the polar radius of the oblate Earth geometry; the inertial longitude of the vehicle position is $\Theta_I = \tan^{-1}(Y_I/X_I)$, the relative longitude with respect to Earth is $\Theta_R = \Theta_I - \Omega_E t$, and the Earth rotation rate, $\Omega_E = 7.29211 \times 10^{-5}$ rad/s. The altitude of the vehicle in Fig. 3 is $h = r_I - R_S$. The radius of the Earth corresponding to $\Phi_{GC}$ is

$$
R_S = \frac{R_E}{\sqrt{1 + \left\{\left(\frac{R_E}{R_P}\right)^2 - 1\right\} \sin^2 \Phi_{GC}}},
$$

the equatorial radius $R_E = 6378.1656$ km and the polar radius, $R_P = 6356.7838$ km. The launch station longitude of ($\Theta$) 80.23621°, geodetic launch latitude of ($\Phi_{GD}$) 13.73204° and launch azimuth of ($A_z$) 102°E are used in the current studies.

The transformation matrix $[T_{LB}]$, which transfers the components of a vector from LPI frame to body frame, is

$$
[T_{LB}] = \{b_{ij}\}_{3\times 3}, \tag{10}
$$

where

$$
\begin{aligned}
b_{11} &= \cos \phi_0 \cos \theta_0 + \sin \phi_0 \sin \Psi_0 \sin \theta_0,\\
b_{12} &= \sin \phi_0 \cos \Psi_0,\\
b_{13} &= -\cos \phi_0 \sin \theta_0 + \sin \phi_0 \sin \Psi_0 \cos \theta_0,\\
b_{21} &= -\sin \phi_0 \cos \theta_0 + \cos \phi_0 \sin \Psi_0 \sin \theta_0,\\
b_{22} &= \cos \phi_0 \cos \Psi_0,\\
b_{23} &= \sin \phi_0 \sin \theta_0 + \cos \phi_0 \sin \Psi_0 \cos \theta_0,\\
b_{31} &= \cos \Psi_0 \sin \theta_0,\\
b_{32} &= -\sin \Psi_0
\end{aligned}
$$

and

$$
b_{33} = \cos \Psi_0 \cos \theta_0.
$$

Here $\psi_0$, $\theta_0$, $\phi_0$ are the initial Euler angles. It should be noted that the transformation matrix, $[T_{LB}]$, which transfers the components of a vector from the CBI frame to body frame, is nothing but the transformation matrix $[T_{LB}]$ having the elements as a function of the sequence of rotation with Euler angles $\psi$, $\theta$, and $\phi$.

The gravitational acceleration along the body frame, $\mathbf{g} = g_x \mathbf{i}_b + g_y \mathbf{j}_b + g_z \mathbf{k}_b$ computed using the transformation matrices $[T_{EL}]$ and $[T_{LB}]$. The components of the gravity forces in the body frame are:

$$
\begin{Bmatrix} g_x \\ g_y \\ g_z \end{Bmatrix} = [T_{LB}][T_{EL}] \begin{Bmatrix} g_{XI} \\ g_{YI} \\ g_{ZI} \end{Bmatrix}. \tag{11}
$$

The gravity force and moment are computed as

$$\mathbf{F}_g = m\mathbf{g}, \tag{12}$$

$$\mathbf{M}_g = \mathbf{r}_{\mathrm{CG}} \times \mathbf{F}_g, \tag{13}$$

where $\mathbf{r}_{\mathrm{CG}} = X_{\mathrm{CG}}\mathbf{i}_b + Y_{\mathrm{CG}}\mathbf{j}_b + Z_{\mathrm{CG}}\mathbf{k}_b$, is the position vector of the vehicle at the center of mass of the vehicle. In general, the center of gravity does not coincide with the center of mass of the vehicle. The gravitational forces will cause moment about the center of mass of the vehicle. However, vehicle dimensions are very small compared to the distance from the Earth center, the moment due to gravitational forces is small compared to other moments.

### 2.3. Force and moment of helical compression springs

The motion of a satellite separating from its final rocket stage by the force of helical compression springs is considered. The separation impulse is provided by release of the energy stored in the helical compression springs. The forward ends of each spring bear against a centering spring cup on the satellite and, since the springs are laterally stable, no auxiliary guides are used. Spring location and support hardware design are dictated by the geometry requirements. To compensate undesirable forces and moments in two axes, the present formulation is based on symmetrically located '$n$'—number of springs. Proper calibration, marking, and grouping of springs as pairs has to be followed to minimize tip off errors due to tolerances and nonlinearity in individual spring characteristics.

The $Z$ component of the spring mounting location in each body is computed as follows (see Fig. 4): $Z_M = L_{MCG}$–$M_{\mathrm{AXIAL}}$ and $Z_S = L_{MCG}$–$S_{\mathrm{AXIAL}}$. Here $Z_M$ is the location of main body CG, $L_{MCG}$ is the location of main body CG from nose cone, $M_{\mathrm{AXIAL}}$ is the axial location of spring mounting with respect to main body, $Z_S$ is the location of the separating body CG, and $S_{\mathrm{AXIAL}}$ is the axial location of spring mounting with respect to separating body. The radial component of spring mounting along $X$ and $Y$ axes are calculated as $r_S \cos\delta$ and $-r_S \sin\delta$, where ($r_S$) is the radial location (m) of the spring from the CG of the individual bodies and $\delta$ is the spring mounting azimuth angle (deg) measured in anticlockwise direction from $P+$ axis. Each of the spring is identified with spring stiffness (i.e. the force required to compress unit length of the spring), free length, and compressed length. The springs on releasing energy will generate forces along the line joining the two ends of the springs. These forces will generate moments about their respective body CGs. In theory, separation may be effected by a large, single compression spring centrally located, but in practice it is usual to use a large number of smaller springs located symmetrically around the periphery. This is preferred firstly for ease of accommodation and secondly to minimize the possibility of a separation aborting through spring failure. The spring force and moments are given by

$$\mathbf{F}_S = \sum_{j=1}^{n} \mathbf{F}_{Sj}, \tag{14}$$

$$\mathbf{M}_S = \sum_{j=1}^{n} \left(\mathbf{r}_{Sj} \times \mathbf{F}_{Sj}\right), \tag{15}$$

where $\mathbf{r}_{Sj} = X_{Sj}\mathbf{i} + Y_{Sj}\mathbf{j} + Z_{Sj}\mathbf{k}$, is the position vector of the $j$th spring location, and $F_{Sj} = -\kappa\xi\cos(f_S t)\mathbf{k}$; $\kappa$ is the spring stiffness and $\xi$ is the stroke length. The frequency of the spring $f_S = 1/2\pi\sqrt{n\kappa/m^*}$, $m^* = m_M m_S/(m_M + m_S)$, is the reduced mass. $m_M$ is the mass of the ongoing body (satellite) and $m_S$ is the mass of the separating (spent) body.

### 2.4. Separation dynamic analysis

It is necessary for separation dynamic analysis to simulate the trajectories of separating bodies taking into account of the forces and moments acting on the bodies. Critical points will be identified on these bodies to estimate the clearances between them. For the identification of collision hazards during separation, the relative

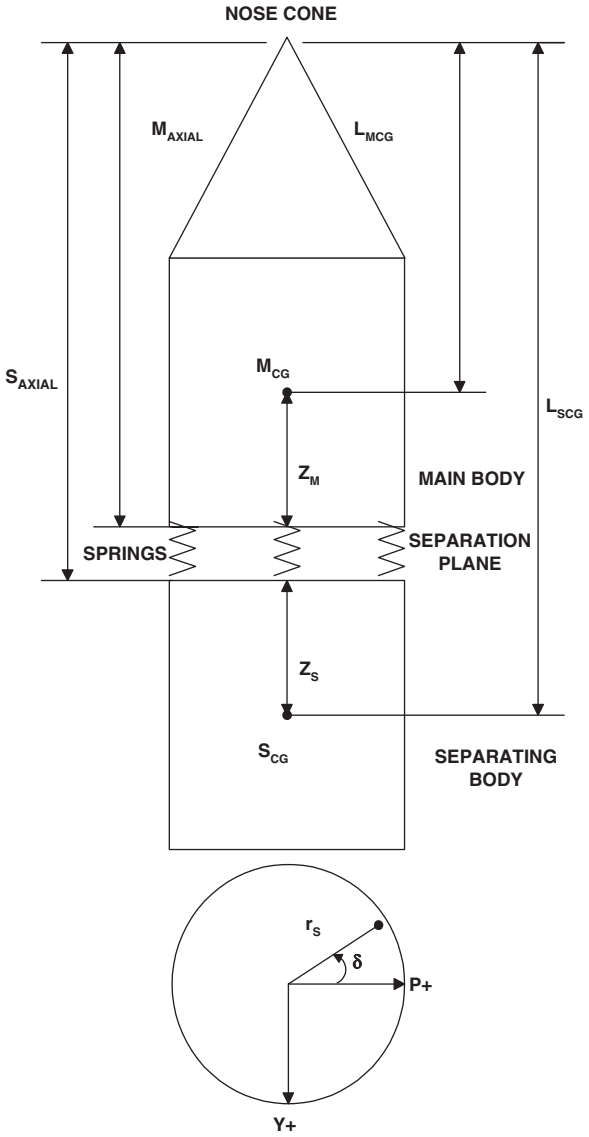


Fig. 4. Springs mounted at the separation plane.

distance between the critical points, relative velocity, body angular velocity and body orientation angles will be estimated. The trace of the points together with body orientation angles will confirm collision-free separation and build up of any tip-off errors on the ongoing functional stage.

Using Eqs. (12)–(15), the total external force and moment vectors in equations of motion (1) and (2) are written as

$$\mathbf{F}_{\text{ext}} = \mathbf{F}_g + \mathbf{F}_S, \tag{16}$$

$$\mathbf{M}_{\text{ext}} = \mathbf{M}_g + \mathbf{M}_S. \tag{17}$$

With these forces and moments, the solution of equations of motion will give the dynamic characteristics of the individual bodies undergoing separation.

After determining the velocities of the individual bodies at a time '$t$', the relative velocity between the separating bodies in the body frame is calculated. Applying the inverse transformation to the relative velocity and integrating with respect to time, the actual separation distance between the bodies is found.

The magnitude of the body rate is

$$|\boldsymbol{\omega}| = \sqrt{r^2 + q^2 + p^2}. \tag{18}$$

The relative velocity ($v_R$) of the separating bodies is:

$$v_R = \sqrt{(v_{x1} - v_{x2})^2 + (v_{y1} - v_{y2})^2 + (v_{z1} - v_{z2})^2}. \tag{19}$$

The relative distance ($d_R$) from the CGs (or) the points identified at the separation plane of the separating bodies is

$$d_R = \sqrt{(x_1 - x_2)^2 + (y_1 - y_2)^2 + (z_1 - z_2)^2}. \tag{20}$$

Here ($v_{x1}$, $v_{y1}$, $v_{z1}$), ($x_1$, $y_1$, $z_1$), ($v_{x2}$, $v_{y2}$, $v_{z2}$) and ($x_2$, $y_2$, $z_2$) are the components of the velocity vector and position vector of the ongoing and spent body which were transformed to CBI frame. The integration of the equations of motion is continued till the spring relaxation time reaches 1/4th of the period. To account the variations in the dynamic parameters, statistical analysis is essential.

## 3. Statistical analysis

In launch vehicle separation system design process, it is with the combination of many variable parameters. For this purpose a multivariate concept, which involves more variable parameters, will be more useful.

Let the variable function be denoted as $\Psi$. The variable $\Psi$ be functionally related to '$n$' random variables, namely, $x_1$, $x_2 \ldots x_n$. This function is assumed to be continuous and differentiable. It can be expressed into a Taylor series about a particular point say $x_1^*, x_2^*, \ldots x_n^*$. Neglecting terms of higher order and assuming that the random variables are independent with means at $x_1^*, x_2^*, \ldots x_n^*$, respectively, the expected (average) value of the function $\Psi$ is approximately given by

$$E(\Psi) \approx \Psi(x_1^*, x_2^*, x_3^*, \ldots, x_n^*) + \frac{1}{2}\sum_{i=1}^{n} \mathrm{Var}(x_i)\frac{\partial^2 \Psi}{\partial x_i^2}. \tag{21}$$

And the variation of the function, $\Psi$ is approximately given by

$$\mathrm{Var}(\Psi) \approx \sum_{i=1}^{n} \mathrm{Var}(x_i)\left(\frac{\partial \Psi}{\partial x_i}\right)^2. \tag{22}$$

The partial derivatives of $\Psi$, in Eqs. (21) and (22) are taken at the point $x_1^*, x_2^*, \ldots x_n^*$, and thus are constants. Further more, if the $x_i$'s are normally distributed, $\Psi$ is approximately normally distributed [24].

If the tolerances of the individual variables all fall with in their specification limit, then the tolerances for the function, $\Psi$ with 99.9% confidence level will not exceed $E(\Psi) \pm 3\sqrt{\mathrm{var}(\Psi)}$. The square root of the variance of a quantity is the standard deviation of that quantity.

In the present study there are 12 variable functions namely velocity components ($v_x$, $v_y$, $v_z$), position components ($x$, $y$, $z$), body rates or angular velocity ($r$, $q$, $p$) and body attitude or orientation components ($\psi$,$\theta$, $\phi$). These variable functions are related to the dynamic parameters of the separating bodies like mass, moment of inertia, CG offset, spring stiffness, spring stroke length, etc. For the variations in the specified dynamic parameters, the above-described statistical analysis will be useful to find the expected value and variance of the 12 variable functions for the ongoing and spent body. With these values, body rate for ongoing and spent body, relative velocity and relative distance between the separating bodies can be estimated. Finally it is possible to estimate the tolerances of the physical quantities.

## 4. Numerical results

Satellite separation system with spring elements between stages is examined here. A simple and reliable statistical approach is employed to obtain tolerance in the magnitude of body rates, relative velocity and relative distance between the separating bodies.

Numerical analysis has been carried out to estimate the tip off rates for the final stage of a multistage rocket carrier for a typical two-tone class geosynchronous transfer orbit. Twelve numbers of helical compression springs having constant stiffness ($\kappa$) of 9360 $\pm$ 3% N/m and the stroke length ($\xi$) of 93.8 $\pm$ 3% mm are specified. Tables 1 and 2 give the trajectory and dynamic parameters reported in the Ref. [23] for the separating bodies at the time of separation. A fourth-order Runge–Kutta integration scheme is used to solve the nonlinear ordinary differential equations with a fixed step size. To simplify the integration process, the time variable in the differential equations is normalized with the spring relaxation time of 1/4th of the period. Components of '$I$', in Eq. (3) are normalized by taking the maximum value of the components as a common factor.

A convergence study has been made by integrating the differential equations with different fixed step sizes for the nominal dynamic parameters of the ongoing body. The results are presented in Table 3. They converge with relative error less than about 1%. Further reducing the integration step size, it is observed that there is no change in the results up to four decimal points. In the present analysis, numerical integration has been carried out with a fixed step size of 0.001.

For the variations in the dynamic parameters, statistical analysis has been performed and presented the expected value and standard deviation of the 12 dof of the separating bodies in Table 4. Utilizing the statistical data of Table 4, the magnitude of the body rate ($|\boldsymbol{\omega}|$), relative velocity ($v_R$) of the separating bodies as well as the relative distance ($d_R$) from the points identified at the separation plane of the separating bodies are evaluated.

The expected value of the body rates for the ongoing and spent bodies are found to be 1.49762 and 1.02737°/s, respectively. The desirable body rate is less than 2°/s. The maximum values of the body rates for these separating bodies are found to be 4.55899 and 2.65991°/s. The body rate of the separated satellite is found to be higher than the desired body rate. The spacecraft CG offset and variations in the spring stiffness may lead to higher body rates, which can be controlled by providing differential springs in the spring system

Table 1
Trajectory parameters at the time of separation

| | |
|---|---|
| Time of separation '$t$' (s) | 1175 |
| Altitude of separation '$h$' (km) | 235 |
| ECI position $X_I$, $Y_I$, $Z_I$ (m) | −5.04096e + 6, 4.2639e + 6, −3.63485e + 5 |
| Initial body rate $r$, $q$, $p$ (deg/s) | −0.0244915, 0.0863901, −0.00900853 |
| Initial attitude $\psi_0$, $\theta_0$, $\phi_0$ (deg) | 1.06252, 142.173, −0.0716475 |
| Body rate assumed for both the bodies due to separation system disturbance (deg/s) | 2 |

Table 2
Dynamic parameters of the separating bodies

| Parameters | Ongoing body | Spent body |
|---|---|---|
| Mass (kg) | 1582.6 ± 16 | 3200 ± 50 |
| $Z$ (mm) | 5804.2 ± 5 | 12258 ± 150 |
| $Y$ (mm) | 18.2 ± 2.5 | 44.6 ± 40 |
| $X$ (mm) | 1.0 ± 2.5 | −72.7 ± 40 |
| $I_{ZZ}$ (kg m$^2$) | 809 ± 5 | 3734 ± 10% |
| $I_{YY}$ (kg m$^2$) | 769 ± 5 | 32416 ± 10% |
| $I_{XX}$ (kg m$^2$) | 663 ± 5 | 32741 ± 10% |
| $I_{XY}$ (kg m$^2$) | −24 ± 15 | −17 ± 100% |
| $I_{XZ}$ (kg m$^2$) | −7 ± 15 | 179 ± 100% |
| $I_{YX}$ (kg m$^2$) | −24 ± 15 | −17 ± 100% |
| $I_{YZ}$ (kg m$^2$) | 11 ± 15 | −414 ± 100% |
| $I_{ZY}$ (kg m$^2$) | 11 ± 15 | −414 ± 100% |
| $I_{ZX}$ (kg m$^2$) | −7 ± 15 | 179 ± 100% |

Table 3
Convergence studies on the solution of differential equations utilizing the nominal dynamic parameters for the ongoing body

| Integration step size | $v_x$ (m/s) | $v_y$ (m/s) | $v_z$ (m/s) | $x$ (m) | $y$ (m) | $z$ (m) | $r$ (°/s) | $q$ (°/s) | $p$ (°/s) | $\theta$ (deg) | $\psi$ (deg) | $\phi$ (deg) |
|---|---|---|---|---|---|---|---|---|---|---|---|---|
| 0.1 | 1.3539 | −0.4333 | 0.4792 | 0.0945 | −0.0110 | 4.3590 | 3.6326 | 0.0600 | 0.0239 | 1.5102 | 142.1836 | −0.0690 |
| 0.01 | 1.3719 | −0.4355 | 0.4773 | 0.1032 | −0.0120 | 4.3621 | 3.6331 | 0.0600 | 0.0239 | 1.5248 | 142.1836 | −0.0689 |
| 0.001 | 1.3764 | −0.4360 | 0.4768 | 0.1045 | −0.0122 | 4.3626 | 3.6331 | 0.0600 | 0.0240 | 1.5274 | 142.1836 | −0.0688 |

Table 4
Variations in 12 degrees of freedom for the separating bodies

| Physical quantities | Ongoing body | | Spent body | |
|---|---|---|---|---|
| | Expected value | Standard deviation | Expected value | Standard deviation |
| $v_x$ (m/s) | 1.37196 | 0.01089 | 1.36914 | 0.00609 |
| $v_y$ (m/s) | −0.28197 | 0.05270 | −0.16397 | 0.02479 |
| $v_z$ (m/s) | 0.4754 | 0.00373 | −0.49118 | 0.00282 |
| $x$ (m) | 0.10321 | 0.00102 | 0.10321 | 0.00092 |
| $y$ (m) | −0.01211 | 0.00012 | −0.01219 | 0.00012 |
| $z$ (m) | 4.36191 | 0.00173 | −2.18456 | 0.05 |
| $r$ (deg/s) | 1.49115 | 1.0214 | 0.06419 | 0.66693 |
| $q$ (deg/s) | 0.06009 | 0.11469 | −0.04549 | 0.02467 |
| $p$ (deg/s) | 0.02311 | 0.01022 | −0.00173 | 0.00587 |
| $\psi$ (deg) | 1.21645 | 0.10326 | 1.05495 | 0.10136 |
| $\theta$ (deg) | 142.18363 | 0.011 | 142.17345 | 0.00236 |
| $\phi$ (deg) | −0.06893 | 0.00099 | −0.07131 | 0.00057 |

assembly. Springs of low and high energy should be assembled in such a way that net spring energy passes through the CG of the spacecraft and nullify the effect due to CG offset on the separated satellite.

For the variations specified in the dynamic parameters the expected values of $v_R$ and $d_R$ are found to be 0.97488 m/s and 6.54609 m, respectively. The tolerances in $v_R$ at 99.9% confidence level are from 0.94954 to 1.00023 m/s, whereas in $d_R$ these are from 6.39599 to 6.69618 m. It should be noted that the distance between the CG's of the separating bodies at time $t = 0$ is 6.4538 m, whereas at the time of spring relaxation time the expected distance is 6.54609 m. The difference between these distances is 92 mm, which is nothing but the gap between the two separating bodies at the time of spring relaxation. This information is essential to the design while selecting the helical compression spring system. The solution of the problem described above corresponds to the short-term dynamics. To examine the collision-free separation in the atmosphere it is essential to specify the forces acting on the separating bodies for further integration beyond the spring relaxation time, which is generally followed in long-term dynamic analysis.

## 5. Conclusions

Dynamics of satellite separation system analysis has been carried out considering the typical multistage rocket carrier. A statistical method is followed to study the influence of design variables on the tip off parameters of the separating bodies. Tolerances on the relative velocity of the separating bodies using the helical compression spring system are found for a geosynchronous transfer orbit. It is noted that the maximum body rate of the separated satellite is found to be higher than the desirable body rate for the specified design variables. To minimize the satellite body rate, it is necessary to employ alternate schemes like changing the spring system combination for controlling CG offset and tightening the other specifications.

## Acknowledgments

The authors would like to thank the reviewers for their valuable suggestions to improve the clarity of this paper.

## References

[1] R.A. Wasko, Experimental investigation of stage separation aerodynamics, NASA Technical Note (NASA-TND-868), National Aeronautics and Space Administration, Washington, DC, May 1961.
[2] W. Chubb, The collision boundary between the two separating stages of the SA-4 Saturn Vehicles, NASA Technical Note (NASA-TND-598), National Aeronautics and Space Administration, Washington, DC, August 1961.
[3] M. Dwork, Coning effects caused by separation of spin stabilized stages, *AIAA Journal* 1 (11) (1963) 2639–2640.
[4] R.O. Wilke, Comments on coning effects caused by separation of spin stabilized stages, *AIAA Journal* 2 (7) (1964) 1358.
[5] J.P. Decker, P.K. Pierpont, Aerodynamic separation characteristics of conceptual parallel-staged reusable launch vehicle at Mach 3 to 6, NASA Technical Memorandum (NASA-TMX-1051), National Aeronautics and Space Administration, Washington, DC, January 1965.
[6] J.P. Decker, Aerodynamic abort-separation characteristics of a parallel staged reusable launch vehicle from Mach 0.60 to 1.20, NASA Technical Memorandum (NASA-TMX-1174), National Aeronautics and Space Administration, Washington, DC, November 1965.
[7] K.J. Ball, G.F. Osborne, *Space Vehicle Dynamics*, Oxford University Press, Oxford, 1967 pp. 59–61.
[8] J.P. Decker, J. Gera, An exploratory study of parallel–stage separation of reusable launch vehicles, NASA Technical Note (NASA-TND-4765), National Aeronautics and Space Administration, Washington, DC, 1968.
[9] A.P. Waterfall, A Theoretical study of the multi-spring stage separation system of the black arrow satellite launcher, Royal Aerospace Establishment, TR-682016, Farnborough Hants, UK, August 1968.
[10] D.R. Longren, Stage separation dynamics of spin stabilized rockets, *Journal of Spacecraft and Rockets* 7 (4) (1970) 434–439.
[11] M.J. Hurley Jr., G.W. Carrie, Stage separation of parallel-staged shuttle vehicles: a capability assessment, *Journal of Spacecraft and Rockets* 9 (10) (1972) 764–771.
[12] K.J. Orlik-Rukemann, S. Iyengar, Example of dynamic interference effects between two oscillating vehicles, *Journal of Spacecraft and Rockets* 10 (9) (1973) 617–619.
[13] J.D.A. Subramanyam, Separation dynamics analysis for a multistage rocket, in: S. Kobayashi (Ed.), *Proceedings of the International Symposium of Space Science and Technology*, AGNE Publishing, Tokyo, 1973, pp. 383–390.
[14] J.P. Decker, A.W. Wilhite, Technology and methodology of separating two similar size aerospace vehicles within the atmosphere, AIAA paper 75-29, AIAA 13th Aerospace Sciences Meeting, Pasadena, CA, January 1975.
[15] K.K. Biswas, Some aspects of jettisoning dynamics related to launch vehicles, in: K.B. Bhatnagar (Ed.), *Space Dynamics & Celestial Mechanics*, Holland, Reidel, 1986, pp. 369–379.
[16] P. Moraes Jr., F. Zdravistch, J.L.F. Azevedo, Aerodynamics of the Brazilian satellite launch vehicle (VLS) during first stage separation, AIAA paper 90-3098, AIAA Eighth Applied Aerodynamics Conference, Portland, Oregon, August 1990.
[17] R. Lochan, V. Adimurthy, K. Kumar, Separation dynamics of strap-on boosters, *Journal of Guidance, Control and Dynamics* 15 (1) (1992) 137–143.
[18] R. Lochan, Dynamics of Bodies Separating from Launch Vehicles, PhD Dissertation, Department of Aerospace Engineering, Indian Institute of Technology, Kanpur, May 1993.
[19] R. Lochan, V. Adimurthy, K. Kumar, Separation dynamics of ullage rockets, *Journal of Guidance, Control and Dynamics* 17 (3) (1994) 426–434.
[20] R. Lochan, V. Adimurthy, Separation dynamics of strap-on boosters in the atmosphere, *Journal of Guidance, Control and Dynamics* 20 (4) (1997) 633–639.
[21] S.C. Cheng, Payload fairing separation dynamics, *Journal of Spacecraft and Rockets* 36 (4) (1999) 511–515.
[22] S. Choi, C. Kim, O.-H. Rho, J.-J. Park, Numerical analysis on separation dynamics of strap-on boosters in the atmosphere, *Journal of Spacecraft and Rockets* 39 (4) (2002) 439–446.
[23] D. Jeyakumar, K.K. Biswas, SPECTRA: separation dynamic simulator for launch vehicles an object oriented approach, in: G. Gurusamy, S. Subharani, R. Neelaveni (Eds.), *Systems Engineering Approach to Sustained Growth*, Proceedings of the 25 National Systems Conference held at PSG College of Technology, Coimbatore, India, December 13–15, 2001. Allied Publishers Limited, New Delhi, 2001, pp. 26–34.
[24] A.H. Bowker, G.I. Lieberman, *Engineering Statistics*, Prentice Hall, Inc, Englewood, Cliffs, NJ, 1972.